Methane dynamics regulated by microbial community response to permafrost thaw

Carmody K. McCalley[1†‡], Ben J. Woodcroft[2], Suzanne B. Hodgkins[3], Richard A. Wehr[1], Eun-Hae Kim[4], Rhiannon Mondav[2†], Patrick M. Crill[5], Jeffrey P. Chanton[3], Virginia I. Rich[4], Gene W. Tyson[2], and Scott R. Saleska[1‡]

[1]Department of Ecology and Evolutionary Biology, University of Arizona, Tucson, AZ, 85721, USA

[2]Australian Centre for Ecogenomics, School of Chemistry and Molecular Biosciences, University of Queensland, Brisbane, 4072, Australia.

[3]Department of Earth, Ocean and Atmospheric Science, Florida State University, Tallahassee, FL, 32306, USA

[4]Department of Soil, Water and Environmental Science, University of Arizona, Tucson, AZ, 85721, USA

[5]Department of Geological Sciences, Stockholm University, Stockholm 106 91, Sweden

[†]Present address: Earth Systems Research Center, University of New Hampshire, Durham, NH, 03824, USA (C.K.M). Department of Ecology and Genetics, Uppsala University, Uppsala 75 236, Sweden (R.M)

[‡]Corresponding authors. Email: carmody.mccalley@unh.edu (C.K.M), saleska@email.arizona.edu (S.R.S)

Permafrost contains approximately 50% of global soil carbon[1]. It is thought that permafrost thaw can lead to soil carbon loss in the form of methane and carbon dioxide emissions[2,3]. The magnitude of the resulting positive climate feedback of such greenhouse

gas emissions remains uncertain[3] and may to a large extent depend on the poorly understood role of microbial community composition in regulating the metabolic processes that drive such ecosystem-scale greenhouse gas fluxes. Here we use a natural landscape gradient of permafrost thaw in northern Sweden[4,5], as a model to investigate the role of microbial communities in regulating methane cycling, and to test whether knowledge of community dynamics could improve predictions of carbon emissions under permafrost loss. We find that changing vegetation and increasing methane emissions with permafrost thaw are associated with a switch from hydrogenotrophic to partially acetoclastic methanogenesis, resulting in a large shift in the $\delta^{13}C$ signature (10-15‰) of emitted methane. Abundance of the methanogen, *Candidatus* Methanoflorens stordalenmirensis[6], is a key predictor of the methane isotope shifts, which in turn predicts the proportion of carbon emitted as methane versus carbon dioxide, an important factor for simulating the climate feedback associated with permafrost thaw in global models[3,7]. By showing that the abundance of key microbial lineages can be used to predict atmospherically relevant patterns in methane isotopes and the proportion of carbon metabolized to methane during permafrost thaw, we establish a basis for scaling changing microbial communities to ecosystem isotope dynamics. Our findings suggest that microbial ecology can play an important role in the ecosystem scale responses to global change.

Multiple factors—including hydrology, vegetation, organic matter chemistry, pH, and soil microclimate—are affected by permafrost loss[5,8,9]. Together these factors regulate microbial metabolisms that release carbon dioxide (CO_2) and methane (CH_4) from thawing permafrost[10–12], and are the basis for earth system model predictions of future CH_4 emissions[7,13,14]. However, the

47 role of microbial community composition in regulating the metabolic processes that drive
48 ecosystem-scale fluxes is unknown.

49 At our study site in Stordalen, as in other thawing permafrost peatlands[8,15], permafrost
50 loss causes hydrologic and vegetation shifts: well-drained permafrost-supported palsas collapse
51 into partially-thawed moss-dominated (*Sphagnum* spp.) bogs and fully-thawed sedge-dominated
52 (e.g. *Eriophorum angustifolium*) fens[4]. Between 1970 and 2000, 10% of Stordalen's palsa habitat
53 thawed into such wetlands[4]. This transition drives an appreciable global warming impact because
54 CO_2-emitting palsa is converted to bogs and fens which take up CO_2 but emit CH_4 (a more
55 potent greenhouse gas[3])[4,5,16]. The net effect is that the high methane-emitting fen contributes 7
56 times the greenhouse impact per unit area as the palsa. This thaw progression is also associated
57 with an increase in overall organic matter lability, including a decrease in C:N and an increase in
58 humification rates[9]. We hypothesized, consistent with previous studies of *in situ* bog and fen
59 systems[17–19], that thaw progression also facilitates a shift from hydrogenotrophic to acetoclastic
60 CH_4 production.

61 We used the distinct isotopic signatures of different microbial CH_4 production and
62 consumption pathways to directly relate changes in CH_4 dynamics across the thaw gradient to
63 underlying changes in the microbial community. Methane produced by hydrogenotrophic
64 methanogens generally has lower $\delta^{13}C$ and higher δD ($\delta^{13}C$ = -110 to -60‰ and δD = -250 to -
65 170‰) relative to that produced by acetoclastic methanogens ($\delta^{13}C$ = -60 to -50‰ and δD = -400
66 to -250‰)[19,20]. If methanotrophic microbes then oxidize CH_4, lighter molecules are
67 preferentially consumed, leaving the remaining CH_4 ^{13}C- and D-enriched relative to the original
68 CH_4 pool (see expected patterns in Extended Data Fig 1)[19,20].

High temporal-resolution measurements of the magnitude and isotopic composition of CH_4 emissions, using a quantum cascade laser spectrometer (QCLS, Aerodyne Research Inc.) connected to autochambers, showed that CH_4 emissions and their ^{13}C content increased with thaw. Average CH_4 fluxes increased from effectively zero at the intact permafrost palsa site to 1.46 ($\pm$0.37) mg CH_4 m^{-2} h^{-1} at the thawing *Sphagnum* site, to 8.75 ($\pm$0.50) mg CH_4 m^{-2} h^{-1} at the fully thawed *Eriophorum* site (Fig. 1a, $p < 0.001$). The average $\delta^{13}C$ of emitted CH_4 also increased significantly, from -79.6‰ ($\pm$0.9) in the *Sphagnum* site to -66.3‰ ($\pm$1.6) in the *Eriophorum* site (Fig. 1b, $p= 0.03$). This consistent 10-15‰ divergence between sites was maintained through the growing season but overlain by parallel fluctuations in $\delta^{13}C$-CH_4, suggesting that weather patterns exerted a common influence over the magnitude of isotopic fractionation. Porewater CH_4 isotopes showed a similar pattern, with *Eriophorum* site porewater $\delta^{13}C$ ~10‰ higher than *Sphagnum* (July and August, Fig. 1b, Extended Data Table 1). Porewater CH_4 was ^{13}C-enriched by 5-20‰ relative to emitted CH_4, as expected due to diffusive fractionation (Methods equation (2)) [18,21].

The apparent fractionation factor for carbon in porewater CH_4 relative to CO_2, α_C (Methods equation (2), Extended Data Table 1), is a related index of changes in CH_4 production[22]. Greater fractionation is associated with hydrogenotrophic methanogenesis, and was found in the thawing *Sphagnum* site (average $\alpha_C = 1.053 \pm 0.002$). Significantly less fractionation ($p=0.002$) associated with more acetoclastic production or with consumption by oxidation was found in the fully thawed *Eriophorum* porewater (average $\alpha_C = 1.046 \pm 0.001$). Here, increases in acetoclastic production, not oxidation, best explain isotopic shifts because lower α_C and higher $\delta^{13}C$-CH_4 are accompanied by significantly lower δD-CH_4 (Extended Data Fig. 1, $p< 0.001$)[19]. This is consistent with the pattern of isotopes in CH_4 emissions as well as

incubations of Stordalen peat[9] and studies showing bog-to-fen shifts from hydrogenotrophic to acetoclastic methanogenesis[17–19].

The CH_4 flux and isotope results provide compelling but indirect evidence for changes in CH_4-cycling microbial communities with permafrost thaw. These microbiological changes could be shifts in activity of particular community members or changes in community composition. We examined the role of community composition through 16S rRNA gene amplicon sequencing. All known methanogens belong to a small number of archaeal lineages within the Euryarchaeota[23]. As expected, the shift from CH_4–neutral intact permafrost palsa to CH_4-emitting wetland corresponded to a substantial increase in the relative abundance of methanogenic archaeal lineages (Fig. 1c, Extended Data Table 2,3). In the aerobic palsa and surface *Sphagnum* habitats, methanogens were found in low relative abundance (average <0.6%), while the anaerobic environments of the *Eriophorum* and deeper (below the water table) *Sphagnum* habitats harbored communities with a substantially higher relative abundance of methanogens (20-30%).

More significantly, the abundance of specific methanogenic lineages varied across the thaw gradient (Fig. 1c, Extended Data Table 2) in a manner corresponding to shifts in CH_4 production mechanism inferred from the isotope data (Fig. 1b). At the partially thawed *Sphagnum* site, where CH_4 isotopes were more hydrogenotrophic, the methanogen community was dominated by hydrogenotrophic populations (>=57% of sequences). Members of the genus *Methanobacterium* and close relatives of the recently described hydrogenotroph, Candidatus '*Methanoflorens stordalenmirensis*'[6] (a partial genome of which has also been identified in incubations of Alaksan permafrost[12]), were the most abundant phylotypes. While present, the metabolically versatile *Methanosarcina* (capable of utilizing a wide range of substrates including acetate and hydrogen[24]), was much less abundant, averaging ~15% of the methanogen sequences.

115 At the fully thawed *Eriophorum* site (where isotope signatures shifted towards acetoclastic),
116 members of the obligately acetoclastic genus *Methanosaeta* increased in abundance, comprising
117 approximately one-third of the methanogenic population. The remaining methanogenic
118 community was taxonomically diverse, including lineages present at the *Sphagnum* site as well
119 as an additional hydrogenotrophic genus, *Methanoregula* (Extended Data Table 2). Differences
120 in the functional (hydrogenotrophic versus acetoclastic) composition of the methanogen
121 community between the sites were smallest in October, coinciding with a convergence in $\delta^{13}C$-
122 CH_4 (Fig. 1a and Extended Data Table 2,3).
123 Together, the isotope and microbial sequence data suggest that microbial community
124 shifts drive large, concordant variations in CH_4 isotope biogeochemistry both seasonally and
125 during permafrost thaw, a novel observation at the ecosystem scale. The early successional
126 hydrogenotroph '*M. stordalenmirensis*'[6] dominates methanogenic metabolism in the early stages
127 of thaw, followed by the subsequent emergence of a more diverse methanogen community,
128 including obligate acetoclastic methanogens. This microbial succession provides direct evidence
129 for how changes in ecosystem structure during permafrost thaw (plant succession and increases
130 in organic matter quality[9]) translate into altered CH_4 biogeochemistry.
131 To quantify the effect of this shifting microbial community composition for CH_4 isotopic
132 patterns, we examined the relationships between isotope fractionation (α_C), environmental
133 conditions known or expected to impact methanogenesis, and the relative abundance of specific
134 methanogenic lineages (Extended Data Table 4). Surprisingly, rather than a functional group
135 (such as hydrogenotrophic methanogens), a single organism -- the hydrogenotroph '*M.*
136 *stordalenmirensis*' -- was the best one-variable predictor of isotopic patterns in the field (Fig.
137 2a). Several variables that typically differentiate bogs and fens, including pH and water table

depth[18], were significant predictors of α_C, however, it was the relative abundance of '*M. stordalenmirensis*' that explained both the large range of α_C observed at the *Sphagnum* site (R^2 = 0.7 , $p < 0.001$) as well as patterns across sites ($R^2 = 0.6$, $p < 0.001$). This suggests, contrary to the current practice of focusing on community functional diversity, that an individual microbial lineage can have a disproportionate influence on ecosystem biogeochemistry.

Stepwise regression identified environmental variables (water table depth, peat C:N and peat $\delta^{13}C$) that improved model predictions of α_C (to $R^2 = 0.8$, $p<0.001$). While confirming the central importance of '*M. stordalenmirensis*' in explaining variation in α_C (Extended Data Table 5) this model also supports the hypothesis that organic matter chemistry underlies shifts in CH_4 metabolism[9,25]. Interestingly, the dependence on the abundance of this lineage was evident despite the relative rather than absolute nature of the community composition analysis, and measurement of abundance rather than activity. We hypothesize that direct measures of gene expression or metabolic activity (meta-transcriptomics and –proteomics) will have an even stronger association than community composition data with isotopic signatures.

Further analysis showed that α_C significantly correlates ($R^2 = 0.7$, $p=0.004$) with the large range in CH_4:CO_2 production ratio (0.13-0.84) measured in anaerobic incubations of Stordalen peat (Fig. 2b). Thus it is likely that changes in the proportion of anaerobically mineralized C that ends up as CH_4—a key, but poorly constrained parameter in global CH_4 models[26]—tracks the abundance of '*M. stordalenmirensis* , which acts as an index of the concerted changes in microbial community and organic matter chemistry that together control the efficiency of carbon metabolism.

Incorporating this understanding of the imprint of microbial communities could be critical to (1) improved model prediction of future climate change CH_4 feedbacks and (2)

accurate attribution of the portion of global atmospheric CH_4 change that derives from permafrost thaw. First, in simulating CH_4 cycling, earth system models typically prescribe as fixed the fraction of anaerobically metabolized carbon that becomes CH_4[26]. The lack of a basis for predicting this parameter across ecosystems and in response to climate change limits current modeling efforts (3). Our finding that the CH_4:CO_2 production ratio is highly variable and predictable from isotopic indicators of methanogenic community composition (Fig. 2b) supports improving representation of microbial ecology in models[17,27]. While simulating microbial population dynamics is beyond the scope of current global models, identification of microbial lineages that predict key parameters, such as the CH_4:CO_2 ratio, provides insights that improve simulations of CH_4 biogeochemistry used to estimate global emissions.

Second, atmospheric inversion studies which use CH_4 mixing ratios and isotopes to infer global sources and sinks of atmospheric CH_4 assume that wetland microbial sources are dominated by acetate fermentation (-58 to -65‰), and, critically, that isotopic signatures from biological sources are constant over time[28,29]. In contrast, we observed isotopic compositions that varied across a gradient of permafrost thaw, with hydrogenotrophic methanogenesis estimated to produce ~50–75% of total CH_4 emission at Stordalen (Extended Data Table 6), with $\delta^{13}C$ averaging -80‰ (Fig. 1b). The hydrogenotrophic $\delta^{13}C$ observed at Stordalen and other Arctic wetlands[30], may be a ubiquitous characteristic of thawing permafrost, particularly during thaw stages that generate recalcitrant organic matter[9,25], such as that observed here in the intermediate-thaw *Sphagnum* site.

To test whether these observed thaw-induced changes in microbial metabolism could be relevant for large-scale atmospheric methane dynamics, we used a simple box model of atmospheric mixing (Methods equation (3)) to quantify the effect of different methanogen

184 communities within recently constructed scenarios of CH_4 emission from thawing permafrost[2]
185 (Extended Data Fig. 2a,b). We found that if hydrogenotrophic lineages regulate CH_4 isotope
186 patterns in permafrost thaw generally, as at Stordalen, then projected CH_4 emissions (Fig. 3a)
187 will produce larger reductions in $\delta^{13}C$ of atmospheric CH_4 than expected from current inversion
188 model assumptions that acetoclasts dominate emissions (Fig. 3b, Extended Data Fig. 2c,d). This,
189 in turn would constrain our simple box model to substantially overestimate the amount of CH_4
190 released from thawing permafrost and underestimate emissions from non-wetland sources, most
191 notably fossil fuels (Fig. 3c). The greater the prevalence of hydrogenotrophic lineages in CH_4
192 emissions, the larger will be the overestimate of fluxes from thaw (Fig 3c). The numerical size
193 of the mis-estimation error here is illustrative; state-of-the-art 3D inversion models have spatially
194 resolved constraints that would likely force smaller flux mis-estimation. But the general
195 implication is that microbial effects are sufficiently important that accurate global accounting of
196 the different sources of CH_4 under future climate change can be improved by understanding the
197 microbial community dynamics underlying biological feedbacks in natural systems.
198 By showing that the abundance of key microbial lineages can be used to predict
199 atmospherically relevant patterns in CH_4 isotopes and the proportion of carbon metabolized to
200 CH_4 during permafrost thaw, this work establishes a basis for scaling changing microbial
201 communities to ecosystem and global-scale atmospheric isotope dynamics. It also highlights the
202 central role that microbial ecology can play in ecosystem-scale responses to global change and
203 the benefit of incorporating microbial dynamics into earth system models.
204
205
206

References

1. Tarnocai, C. *et al.* Soil organic carbon pools in the northern circumpolar permafrost region. *Global Biogeochemical Cycles* **23**, GB2023 (2009).

2. Schuur, E. A. G. *et al.* Expert assessment of vulnerability of permafrost carbon to climate change. *Climatic Change* **119**, 359–374 (2013).

3. Ciais, P. *et al.* 2013: Carbon and Other Biogeochemical Cycles. *Climate Change 2013: The Physical Science Basis. Contribution of Working Group I to the Fifth Assesment Report of the Intergovernmental Panel on Climate Change* (2013).

4. Johansson, T. *et al.* Decadal vegetation changes in a northern peatland, greenhouse gas fluxes and net radiative forcing. *Global Change Biology* **12**, 2352–2369 (2006).

5. Christensen, T. R. *et al.* Thawing sub-arctic permafrost: Effects on vegetation and methane emissions. *Geophysical Research Letters* **31**, L04501 (2004).

6. Mondav, R. *et al.* Discovery of a novel methanogen in thawing permafrost. *Nature Communications* (2014).doi:10.1038/ncomms4212

7. Melton, J. R. *et al.* Present state of global wetland extent and wetland methane modelling: conclusions from a model inter-comparison project (WETCHIMP). *Biogeosciences* **10**, 753–788 (2013).

8. Jorgenson, M. T., Racine, C. H., Walters, J. C. & Osterkamp, T. E. Permafrost degradation and ecological changes associated with a warming climate in central Alaska. *Climate Change* **48**, 551–579 (2001).

9. Hodgkins, S. B. *et al.* Changes in peat chemistry associated with permafrost thaw increase greenhouse gas production. *Proceedings of the National Academy of Sciences* **111**, 5819–5824 (2014).

10. Olefeldt, D., Turetsky, M. R., Crill, P. M. & McGuire, A. D. Environmental and physical controls on northern terrestrial methane emissions across permafrost zones. *Global Change Biology* **19**, 589–603 (2012).

11. Lee, H., Schuur, E. A. G., Inglett, K. S., Lavoie, M. & Chanton, J. P. The rate of permafrost carbon release under aerobic and anaerobic conditions and its potential effects on climate. *Global Change Biology* **18**, 515–527 (2012).

12. Mackelprang, R. *et al.* Metagenomic analysis of a permafrost microbial community reveals a rapid response to thaw. *Nature* **05**, (2011).

13. Riley, W. J. *et al.* Barriers to predicting changes in global terrestrial methane fluxes: analyses using CLM4Me, a methane biogeochemistry model integrated in CESM. *Biogeosciences* **8**, 1925–1953 (2011).

14. Koven, C. D. *et al.* Permafrost carbon-climate feedbacks accelerate global warming. *Proceedings of the National Academy of Sciences* **108**, 14769–74 (2011).

15. Turetsky, M. R., Wieder, R. K. & Vitt, D. H. Boreal peatland C fluxes under varying permafrost regimes. *Soil Biology and Biochemistry* **34**, 907–912 (2002).

16. Bäckstrand, K. *et al.* Annual carbon gas budget for a subarctic peatland, Northern Sweden. *Biogeosciences* **7**, 95–108 (2010).

17. Bridgham, S. D., Cadillo-Quiroz, H., Keller, J. K. & Zhuang, Q. Methane emissions from wetlands: biogeochemical, microbial, and modeling perspectives from local to global scales. *Global Change Biology* (2013).doi:10.1111/gcb.12131

18. Hornibrook, E. R. C. & Bowes, H. L. Trophic status impacts both the magnitude and stable carbon isotope composition of methane flux from peatlands. *Geophysical Research Letters* **34**, 2–6 (2007).

19. Chanton, J. P., Chaser, L. C., Glaser, P. & Siegel, D. Carbon and hydrogen isotopic effects in microbial methane from terrestrial environments. *Stable Isotopes and Biosphere-Atmosphere Interactions, Physiological Ecolgy Series* 85–105 (2005).

20. Whiticar, M. J. Carbon and hydrogen isotope systematics of bacterial formation and oxidation of methane. *Chemical Geology* **161**, 291–314 (1999).

21. Popp, T. J., Chanton, J. P., Whiting, G. J. & Grant, N. Methane Stable Isotope Distribution at a Carex Dominated Fen in North Central Alberta. *Global Biogeochemical Cycles* **13**, 1063–1077 (1999).

22. Whiticar, M. J., Faber, E. & Schoel, M. Biogenic methane formation in marine and freshwater environments: CO2 reduction vs. acetate fermentation-Isotope evidence. *Geochimica et Cosmochimica Acta* **50**, 693–709 (1986).

23. Ferry, J. G. How to make a living by exhaling methane. *Annual review of microbiology* **64**, 453–73 (2010).

24. Liu, Y. & Whitman, W. B. Metabolic, phylogenetic, and ecological diversity of the methanogenic archaea. *Annals of the New York Academy of Sciences* **1125**, 171–89 (2008).

25. Hornibrook, E. R. C., Longstaffe, F. J. & Fyfe, W. S. Spatial distribution of microbial methane production pathways in temperate zone wetland soils: Stable carbon and hydrogen isotope evidence. *Geochimica et Cosmochimica Acta* **61**, 745–753 (1997).

26. Wania, R. *et al.* Present state of global wetland extent and wetland methane modelling: methodology of a model inter-comparison project (WETCHIMP). *Geoscientific Model Development* **6**, 617–641 (2013).

27. Wieder, W. R., Bonan, G. B. & Allison, S. D. Global soil carbon projections are improved by modelling microbial processes. *Nature Climate Change* **3**, 909–912 (2013).

28. Kai, F. M., Tyler, S. C., Randerson, J. T. & Blake, D. R. Reduced methane growth rate explained by decreased Northern Hemisphere microbial sources. *Nature* **476**, 194–7 (2011).

29. Bousquet, P. *et al.* Contribution of anthropogenic and natural sources to atmospheric methane variability. *Nature* **443**, 439–43 (2006).

30. Hines, M. E., Duddleston, K. N., Rooney-Varga, J. N., Fields, D. & Chanton, J. P. Uncoupling of acetate degradation from methane formation in Alaskan wetlands: Connections to vegetation distribution. *Global Biogeochemical Cycles* **22**, 1–12 (2008).

Supplementary Information is linked to the online version of the paper at www.nature.com/nature.

Acknowledgements We thank the Abisko Scientific Research Station for infrastructure and logistical support, Tyler Logan and Niklas Rakos for their assistance in the field, and Steve Wofsy and Steve Frolking for feedback on a draft of this paper. This work was supported by the US Department of Energy Office of Biological and Environmental Research (award DE-SC0004632).

Author Contributions S.R.S., V.I.R., P.M.C., J.C. and G.W.T. designed the study. C.K.M., S.B.H., R.A.W., P.M.C., J.C. and S.R.S. designed and/or performed flux/porewater/isotope measurements and laboratory incubations. C.K.M., B.J.W., R.M., E.-H.K., S.R.S., V.I.R. and G.W.T. designed and/or performed analyses integrating bioinformatics and biogeochemistry.

C.K.M., V.I.R., and S.R.S wrote the paper in consultation with B.J.W., S.B.H., J.C., P.M.C., E.-H.K., R.M., and G.W.T.

Author Information Amplicon sequencing data have been deposited in the sequence read archive with accession number SRP042265. Reprints and permissions information is available at www.nature.com/reprints. Correspondence and requests for materials should be addressed to C.K.M (carmody.mccalley@unh.edu) or S.R.S (saleska@email.arizona.edu).

Figure 1. Increases in the magnitude and $\delta^{13}C$ signature of CH_4 during permafrost thaw track shifts in methanogen communities. a, Average daily CH_4 emissions (error bars represent s.e.m, n = 2-3) **b,** $\delta^{13}C$ composition of emitted and porewater CH_4 (error bars represent s.e.m, flux n = 2-3, porewater n = 6-9) and **c,** relative abundance of methanogenic groups as inferred by taxonomic identity assigned from 16S rRNA amplicon sequencing**,** for a permafrost thaw sequence at Stordalen Mire. For the intermediate thaw *Sphagnum* site, aerobic communities were sampled above the water table, anaerobic communities were sampled below the water table.

Figure 2. Correlation between the effective isotopic fractionation of methanogenesis, and both the relative abundance of the methanogen Candidatus '*Methanoflorens stordalenmirensis*', and the anaerobic CH_4:CO_2 production ratio. a, The relative abundance of a single methanogen, Candidatus '*Methanoflorens stordalenmirensis*' was significantly correlated ($p < 0.001$) with porewater effective fractionation (α_C), an isotopic indicator of methanogenic production pathway. **b,** Anaerobic incubations of peat collected from a related thaw sequence at Stordalen Mire (see methods in [9]) show a significant correlation between αC

and the CH_4:CO_2 production ratio, suggesting that the abundance of '*M. stordalenmirensis*' may be indicative of the proportion of organic matter metabolized to CH_4.

Figure 3. Simulated effect of CH_4 from different methanogen communities in thawing permafrost on atmospheric $\delta^{13}C$-CH_4 in a box model of the atmosphere. a, Modeled CH_4 emissions under high (red bounding lines) and low (orange bounding lines) climate warming scenarios, and a range within each (in gray) spanning high and low C release scenarios[2]. The red dashed line is an intermediate emissions scenario used to simulate **b,** consequent reductions in $\delta^{13}C$ of atmospheric CH_4 due to emissions dominated by hydrogenotrophic lineages, as in intermediate-thaw *Sphagnum* sites (green line, $\delta^{13}C$ = -80‰), or more by acetoclasts, as in fully-thawed "*Eriophorum*" sites (blue line, $\delta^{13}C$ = -65‰). Atmospheric inversion models typically assume emissions have $\delta^{13}C$ ranging from = -60 (black line) to -65 (blue line). (The dotted horizontal line indicates the current detection limit for atmospheric CH_4 isotopes[28]). These imply an underestimate of the effect on atmospheric $\delta^{13}C$ for the given emissions scenario (blue or green). In order to match observed atmospheric isotopes, the box model would then require **c**, a corresponding overestimate of CH_4 flux attributed to permafrost thaw (vertical axis). The magnitude of the overestimate depends on the mismatch between model-assumed isotopic composition (upper line = -60‰ , lower line = -65‰), and the actual isotopic composition produced by different communities, which ranges here along the horizontal axis from -80‰ (hydrogenotroph-dominated as in the partially-thawed "*Sphagnum*" sites), to -65‰ (acetoclastic, as in the fully thawed "*Eriophorum*" sites).

Methods

Site Description and permafrost thaw

Stordalen is a sub-arctic palsa mire located 10km east of Abisko in the discontinuous permafrost zone of northern Sweden (68°21'N 18°49'E, altitude 363 m a.s.l.). This work focuses on three distinct subhabitats, common to northern wetlands and together covering ~98% of the Mire surface: (i) permafrost-dominated, well-drained palsas occupied by feather mosses and ericaceous and woody plants, covering 49% of the mire (ii) intermediate permafrost sites with variable water table depth, dominated by *Sphagnum* spp., covering 37% of the mire, and (iii) full summer-thaw, wet sites with *Eriophorum angustifolium,* covering 12% of the mire. Between 1970 and 2000, as permafrost thawed and palsas collapsed, *Sphagnum* sites and *Eriophorum* sites expanded by 3% and 54%, respectively[4].

Formation of wetlands following permafrost thaw, as observed at Stordalen, is a widespread characteristic of peatlands affected by permafrost loss[8,31–33]. Thawing of ice-rich features results in peatland collapse and the formation bogs and fens. At Stordalen, thaw is associated with a progression from ombrotrophic bogs to minerotrophic fens due to thaw-induced subsidence increasing hydrologic connectivity. A similar successional shift from bogs dominated by *Sphagnum* spp. to tall graminoid fens has been observed in other northern peatlands[8,33–35]. More generally, landscape features and hydrologic conditions dictate the characteristics and trajectory of wetland communities formed following permafrost thaw[36]. For example, rapid fen development is observed at the subsiding margins of permafrost plateaus[37], whereas collapse bogs and thermokarst lakes often form within large, thawing peatland complexes[32]. Large uncertainty in model predictions of the extent and characteristics of wetland

363 formation arising from permafrost thaw is a critical limitation to current understanding of
364 carbon-climate feedbacks[7,14]. As demonstrated in this study, improved characterization and
365 modeling of peatland transformation during thaw will be essential for accurately predicting post-
366 thaw microbial communities and the resultant magnitude and isotopic composition of CH_4
367 emissions under climate change.

368 **Methane Isotope systematics**

369 We use standard δ notation for quantifying the isotopic compositions of CH_4 and CO_2:
370 the ratio R of ^{13}C to ^{12}C (or D to H) in the measured sample is expressed as a relative difference
371 (denoted $\delta^{13}C$ or δD) from the Vienna Pee Dee Belemnite (VPDB) international standard
372 material. For example, for C:

373 $$^{13}C = \frac{R \quad R_{VPDB}}{R_{VPDB}} = \frac{R}{R_{VPDB}} \quad 1 \qquad (1)$$

374 $\delta^{13}C$ is often expressed in parts-per-thousand (per mil, ‰).

375 Isotopic fractionation in chemical reactions (including methanogenesis or
376 methanotrophy) or due to diffusion may be quantified as (Farquhar et al., 1989):

377 $$= \frac{R_{source}}{R_{product}} = \frac{_{source} + 1}{_{product} + 1} \qquad (2)$$

378 For diffusive fractionation, R_{source} is taken to be the isotopic ratio in the concentrations of the
379 gradient and $R_{product}$ the ratio in the resultant net flux. Because diffusion discriminates against
380 the heavy isotope, $R_{product} < R_{source}$, which implies, for example, that the isotopic ratio of
381 porewater (the "source") will be greater than that of the flux of gas diffusing out, as we see here
382 (Fig. 1a). Methanogenesis and methanotrophy also discriminate against the heavier isotopes, so

that $R_{product} < R_{source}$ (and hence $\alpha > 1$) for both C and H in methane. Note that $\alpha > 1$ for methanotrophy implies that the products of CH_4 oxidation (CO_2 and H_2O) are lighter (have lower *R*) in both C and H relative to the source CH_4; but mass balance then requires the residual methane not oxidized to become heavier in both C and H, relative to the starting composition of the CH_4 pool before oxidation.

The degree of C isotopic fractionation between CO_2 and CH_4 differs between the two main biochemical pathways of methanogenesis, *acetoclastic* ($CH_3COOH \rightarrow CH_4 + CO_2$) and *hydrogenotrophic* ($CO_2 + 4H_2 \rightarrow 2H_2O + CH_4$). Carbon isotope fractionation (α_C) is greater for hydrogenotrophic than for acetoclastic methanogenesis, but α_H (hydrogen isotope fractionation) follows the opposite pattern: α_H (hydrogenotrophic) < α_H (acetoclastic) (Extended Data Fig. 1; Chanton et al[19]). Hence, variations in C and H isotopic compositions of CH_4 that arise from variations in methanogenic pathway will be anti-correlated: shifts from hydrogenotrophic to acetoclastic production will cause C isotope ratios to increase but H isotope ratios to decline, moving along a negatively-sloped "production line" in H vs C isotope space (Extended Data Fig. 1). Isotopic variations that arise from variations in the degree of methanotrophy, by contrast, will be positively correlated: shifts towards increasing methanotrophy will cause both C and H isotope ratios to increase along a positively sloped "oxidation line" (Extended Data Fig. 1).

In a field study like this one, it is difficult to directly estimate fractionation factors directly; hence, we follow standard practice in the methane biogeochemistry literature (eg. Whiticar et al.[22,38]) and estimate the net or effective fractionation factor from *in situ* pore water data. For example, we estimate α_C, the effective fractionation factor for C in CH_4, by applying equation (2), setting $\delta_{product} = \delta^{13}C_{CH4}$ and $\delta_{source} = \delta^{13}C_{CO2}$, where $\delta^{13}C_{CH4}$ and $\delta^{13}C_{CO2}$ are the

406 observed C compositions of CH_4 and CO_2, respectively[38]. Using CO_2 isotope composition for
407 δ_{source} follows directly for hydrogenotrophic methanogenesis (for which CO_2 is the source C
408 substrate), and has been found to work also in practice for acetoclastic methanogenesis, as
409 porewater CO_2 arises primarily from respiration of organic matter (a non-discriminatory
410 reaction), and so is typically isotopically indistinguishable from organic matter[20,39].
411
412 **Autochamber measurements**

413 The autochamber system at Stordalen mire has previously been described in detail for
414 measurements of CO_2 and total hydrocarbons[16,40]. Briefly, a system of 8 automatic gas-sampling
415 chambers made of transparent Lexan was installed in the three habitat types at Stordalen Mire in
416 2001 (n=3 each in the palsa and *Sphagnum* habitats, and n=2 in the *Eriophorum* habitat). Each
417 chamber covers an area of 0.14 m^2 (38 cm x 38 cm), with a height of 25–45 cm, and is closed
418 once every 3 hours for a period of 5 min. The chambers are connected to the gas analysis system,
419 located in an adjacent temperature controlled cabin, by 3/8" Dekoron tubing through which air is
420 circulated at approximately 2.5 L min^{-1}. During the 2011 season the system was updated with a
421 new chamber design similar to that described by Bubier *et al*[41]. The new chambers each cover an
422 area of 0.2 m^2 (45 cm x 45 cm), with a height ranging from 15-75 cm depending on habitat
423 vegetation. At the Palsa and *Sphagnum* site the chamber base is flush with the ground and the
424 chamber lid (15 cm in height) lifts clear of the base between closures. At the *Eriophorum* site the
425 chamber base is raised 50–60 cm on lexon skirts to accommodate large stature vegetation.
426 Additionally, each chamber is instrumented with thermocouples measuring air and surface
427 ground temperature, and water table depth is measured manually 3–5 times per week. The Palsa
428 site chambers are located within the palsa site in Mondav, Woodcroft et al[6] and correspond to the

hummock site class (I) described in Johansson et al[4]. The *Sphagnum* site chambers are located within the bog site in Mondav, Woodcroft et al[6] or site S in Hodgkins et al[9] and correspond to the semi-wet and wet site class (II and III) described in Johansson et al[4]. The *Eriophorum* site chambers are located within the fen site in Mondav, Woodcroft et al[6] or site E in Hodgkins et al[9] and correspond to the tall graminoid site class (IV) described in Johansson et al[4].

QCLS measurement and calibration

Methane fluxes and isotopes were measured using a Quantum Cascade Laser Spectrometer (QCLS, Aerodyne Research Inc), deployed to Stordalen Mire in June 2011. The QCLS instrument deployed at Stordalen is a modification of the technology described in detail by Santoni et al[42]. Briefly, the QCLS uses a room-temperature continuous wave mid-infrared laser whose frequency was tuned to rapidly (900 kHz) scan across $^{12}CH_4$ and $^{13}CH_4$ absorption lines in the 7.5 μm region. The laser light enters a multipass sample cell (effective path length of ~200m) containing sample air at low pressure (~5 kPa) and is detected by a thermoelectrically cooled detector (no cryogens are needed). Aerodyne Research's custom TDL Wintel software averages high-frequency spectra to produce independent $^{12}CH_4$ and $^{13}CH_4$ mixing ratios in the sample airstream at 1 sec intervals. The ratio, R, of $^{13}CH_4$ to $^{12}CH_4$ and can then be expressed in standard notation as $\delta^{13}C$, the part-per-thousand (per mil, ‰) deviation of the measured ratio from the VPDB standard $^{13}C/^{12}C$ ratio R_{VPDB}, according to equation (1).

Instrument precision in the field at Stordalen Mire was assessed using time-series measurements of calibration tank air over 30–40 min. The precision of $\delta^{13}C$ CH_4 measurements using a 1 second integration time was 1‰. The Allan variance technique (used to characterize the minimum possible measurement error and the averaging time required to achieve it[43]),

showed that the minimum measurement error on $\delta^{13}C\text{-}CH_4$ was <0.2‰ , achieved with 60 seconds of averaging time. This approaches the precision of comparable measurements made using GC-IRMS.

We connected the QCLS to the main autochamber circulation using ¼" Dekoron tubing and a solenoid manifold that enables selection between the autochamber flow and an array of calibration tanks. During measurement periods, filtered (0.45 μm, Teflon filter) and dried (Perma Pure PD-100T-24MSA) sample-air flows at 1.4 slpm through the 2L QCLS sample cell volume at 5.6 kPa. A downstream solenoid controls the QCLS return flow so that air only recirculates during autochamber measurement periods, during calibration periods exhaust air is vented to the room.

Calibrations were done every 60 min using 3 calibration gases spanning the observed concentration range (1.5–10 ppm). The CH_4 concentration and $\delta^{13}C$ composition of each calibration tank was determined by inter-calibration with a set of 4 well-characterized primary standard tanks. The primary tanks (Scott Marin, Inc, Riverside CA) were calibrated to the VPDB scale by means of flask samples, which were analyzed by GC-IRMS at Florida State University (see porewater methods for GC-IRMS details). Each isotopologue, $^{12}CH_4$ and $^{13}CH_4$, was treated as an independent measurement and calibrated separately. For each calibration period a linear calibration curve was fitted for each isotopologue and the fit parameters were then linearly interpolated between calibration periods. The interpolated fit parameters were applied to the measured sample isotopologue mixing ratios to give calibrated measurements of $^{12}CH_4$, $^{13}CH_4$, and total CH_4, from which $\delta^{13}C\text{-}CH_4$, was calculated.

Autochamber data processing

For each autochamber closure we calculated flux and $\delta^{13}C$ signiture of emitted CH_4. Fluxes were calculated using a method consistent with that detailed by Bäckstrand et al[44] for CO_2 and total hydrocarbons, using a linear regression of changing headspace CH_4 concentration over a period of 2.5 min. Eight 2.5 min regressions were calculated, staggered by 15 sec, and the most linear fit (highest r^2) was then used to calculate flux. Keeling plots[45–47] using the entire closure period were used to estimate the isotopic composition of the emitted CH_4. As demonstrated by Santoni *et al*[42], negligible error in measurment of CH_4 relative to that of $\delta^{13}CH_4$ for this instrumentation meant that Type I regression was sufficient for the Keeling plot analysis. When the total change in headspace CH_4 was low[45], there was high error in the Keeling intercept. We used a threshold of 3‰ uncertainty in the Keeling intercept as a cut-off for including isotopic values in the calculation of daily and annual averages, resulting in a total of 1569 observations at the *Sphagnum* site and 1168 at the *Eriophorum* site. No Palsa chamber closures had sufficient CH_4 flux to calculate $\delta^{13}CH_4$. Daily and whole-season average flux and isotopic composition for each habitat were calculated based on individual chambers as the unit of replication (n=3 for Palsa and *Sphagnum*, n=2 for *Eriophorum*). Significant differences in the magnitude and isotopic composition of CH_4 emissions were determined using a Student's t-test (isotopic composition) and ANOVA (flux magnitude) in R[48], with seasonal averages for each auto-chamber as the unit of replication. Statistical significance was determined at $\alpha = 0.05$.

Porewater sampling and analysis

Porewater samples were collected on July 12, 2011, August 15, 2011 and October 15, 2011 at three locations adjacent to the *Sphagnum* and *Eriophorum* auto-chamber sites (Extended Data Table 1). Samples were collected by suction with a syringe through a stainless steel tube and filtered through 25-mm diameter Whatman Grade GF/D glass microfiber filters (2-µm

496 particle retention). Porewater pH was measured in the field (Oakton Waterproof pHTestr 10,
497 Eutech Instruments). Samples for the analysis of the concentration and $\delta^{13}C$ of CH_4 and CO_2
498 were injected into 30-mL evacuated vials sealed with butyl rubber septa and frozen within 8
499 hours of collection. The samples for δD-CH_4 were injected into 120-mL evacuated vials sealed
500 with butyl rubber septa and containing 0.5 g of KOH. For δD-H_2O, water was filtered directly
501 into 2-mL plastic screw cap vials so that the vials were completely filled, then frozen within 8
502 hours of collection. All samples were shipped frozen to Florida State University for analysis.

503 Samples collected for analysis of CH_4 and CO_2 concentrations and $\delta^{13}C$ were thawed,
504 acidified with 0.5 mL of 21% H_3PO_4, and brought to atmospheric pressure with helium. The
505 sample headspace was analyzed for concentrations and $\delta^{13}C$ of CH_4 and CO_2 on a continuous-
506 flow Hewlett-Packard 5890 gas chromatograph (Agilent Technologies) at 40°C coupled to a
507 Finnigan MAT Delta S isotope ratio mass spectrometer via a Conflo IV interface system
508 (Thermo Scientific, Bremen, Germany). The headspace gas concentrations were converted to
509 porewater concentrations based on their known extraction efficiencies, defined as the proportion
510 of formerly-dissolved gas in the headspace. An extraction efficiency of 0.95 (based on repeated
511 extractions) was used for CH_4, and the extraction efficiency for CO_2 relative to DIC was
512 determined based on CO_2 extraction from dissolved bicarbonate standards[49].

513 Samples collected for analysis of δD-CH_4 were brought to atmospheric pressure with
514 helium and measured on a gas chromatograph connected to a ThermoFinnegan Delta Plus
515 continuous flow isotope ratio mass spectrometer at the National High Magnetic Field Laboratory
516 (Tallahassee, FL). δD of CH_4 is affected by δD of H_2O because CH_4 exchanges H atoms with
517 water during methanogenesis [20,38,50], so measurement of δD-H_2O is necessary for correct

assignment of CH_4 production mechanisms and oxidation based on δD and $\delta^{13}C$ of CH_4. Samples collected for δD-H_2O were measured on an LGR DT-100 liquid water stable isotope analyzer at Florida Agricultural and Mechanical University (Tallahassee, FL). Data analysis for these samples was performed using an MS Excel template from the IAEA Water Resources Programme (http://www.iaea.org/water).

Significant differences in α_C and δD and $\delta^{13}C$ of porewater CH_4 between the *Sphagnum* and *Eriophorum* sites were determined using a Student's t-test (α_C, δD-CH_4, $\delta^{13}C$-CH_4) and Hotelling's t-test (multivariate δD and $\delta^{13}C$ of CH_4) in R^{48}. Statistical significance was determined at $\alpha = 0.05$.

Peat sampling

Peat samples were collected on July 12, 2011, August 16, 2011 and October 16, 2011 at three locations adjacent to the Palsa, *Sphagnum* and *Eriophorum* auto-chamber sites. For the *Sphagnum* and *Eriophorum* sites samples were collected at the same depths and locations used for porewater sampling (Extended Data Table 1), sample depths for the Palsa site are detailed in Mondav et al[6]. Peat cores were collected using a 11 cm diameter push corer (Palsa and *Sphagnum* sites) or a 10 cm x 10 cm Wardenaar corer (*Eriophorum* site). Cores were subsampled by depth and were subdivided in the field for microbial and chemical analysis, avoiding the outer 1cm of the core. Samples for microbial analysis were placed in cryotubes, saturated with ~3 volumes LifeGuard solution (MoBio Laboratories, Carlsbad, CA, USA) and stored at -80°C until processing. Samples for chemical analysis were placed in plastic bags and frozen until processing.

Peat chemical analysis

For peat %C, %N, C:N ratio, and $\delta^{13}C$ measurements, 5–10 g of peat was dried at 60 °C until completely dry (3–10 days) and ground to a fine powder. Subsamples of ground peat (80–100 μg for %C and $\delta^{13}C$ analysis, and 5000–6000 μg for %N analysis) were wrapped in tin capsules and analyzed by combustion to CO_2 and N_2 at 1020 °C in an automated CHN elemental analyzer coupled with a ThermoFinnegan Delta XP isotope ratio mass spectrometer at the National High Magnetic Field Laboratory (Tallahassee, FL). Samples were run in non-dilution mode for carbon analysis and dilution mode (×10) for nitrogen analysis. C:N was calculated as the ratio of (%C)/(%N) (by weight) for corresponding pairs of subsamples.

SSU rRNA gene amplicon analysis

Sampling and extraction was carried out as per Mondav et al [6]. Several additional samples were analyzed for this paper, multiplex identifiers for those runs not reported in Mondav et al[6] are provided in Extended Data Table 7. SSU rRNA gene sequences were processed using APP 3.0.3 (https://github.com/Ecogenomics/APP). Homoploymer errors were corrected using Acacia[51] and the resulting reads were processed using the CD-HIT-OTU 0.0.2 pipeline with minor adjustments[52]. All reads were trimmed to 250bp and reads <250bp were discarded. Sequences were clustered at 97% identity and each cluster assigned a taxonomy using BLASTN 2.2.22 [53] through the QIIME script assign_taxonomy.py[54] against the GreenGenes Oct 2012 database clustered at 99% identity (Supplementary Data 1). Each abundant methanogenic cluster's taxonomy was confirmed using parsimony insertion with ARB[55] Amplicon sequence clusters were identified as potential hydrogenotrophic or acetoclastic methanogens based on taxonomic relationship to known methanogenic lineages (Extended Data Table 2)[23,24,56]. Within

564 the order *Methanosarcinales*, lineages most closely related to *Methanosaeta* were classified as
565 obligate acetoclasts, whereas those most closely related to *Methanosarcina* were considered
566 facultative acetoclasts, having the potential for both acetoclastic or hydrogenotrophic
567 production[23].
568
569 **Regression analysis**
570 A step-wise regression approach using Akaike's information criterion (AIC) as the model
571 selection criterion was used to identify a sub-set of microbial and environmental predictor
572 variables that best explained CH_4 metabolism patterns quantified as porewater α_C (Extended Data
573 Table 5). Model selection was done using the stepAIC package in R and the relative importance
574 of the predictor variables in the selected model was then calculated using the relaimpo R package
575 [48]. Variables included in the model selection process included the relative abundance of the 6
576 most abundant methanogen operational taxonomic units (OTUs) (comprising >93% of total
577 methanogen sequences; see Extended Data Table 2) plus soil temperature, water table depth, pH,
578 porewater CH_4 and DIC concentration, and peat C:N, % C, % N and $\delta^{13}C$ (Extended Data Table
579 1). Strong correlation between pH and both water table depth and peat $\delta^{13}C$ as well as peat %N
580 and both %C and C:N meant that pH and %N were excluded from the regression analysis.
581 Removing non-significant predictor variables (DIC and relative abundance of an unidentified
582 *Methanobacterium* spp. (otu-3636, Extended Data Table 2)) had a minimal effect on the model
583 AIC value (<1) and this simplified version was therefore selected as the optimal model (Model 2
584 in Extended Data Table 5). Stepwise regression was also done with $\delta^{13}C$-CH_4 as the dependent
585 variable. This analysis resulted in a similar model outcome, but with a lower R^2 (Model 1 in
586 Extended Data Table 8). Stepwise regression analysis with environmental predictor variables and

587 the relative abundance of the influential methanogen '*M stordalenmirensis*' (otu-10747) as the
588 dependent variable showed that patterns in this methanogen's abundance were influenced by
589 environmental conditions, particularly water table depth and peat chemistry (Model 2 in
590 Extended Data Table 8). These environmental variables alone, however, cannot fully replace
591 microbial data when modeling α_C. Stepwise regression analysis using only environmental
592 variables to predict α_C yielded a model with a lower AIC and R^2 (Model 3 in Extended Data
593 Table 8). It is the combination of methanogen and environmental variables that yields a model
594 that explains the most variability in α_C (Extended Data Table 5).
595
596 **Box Model of atmospheric methane**
597 The model used here was a 1-box model simplified from the 2-box model of Tans[57] (and
598 also used in the Kai et al.[28] methane inversion study):
599
$$\frac{dM}{dt} = F_{CH_4} \quad M \tag{3}$$
$$\frac{d(RM)}{dt} = R_{CH_4}F_{CH_4} - \alpha_{OH}\lambda(RM)$$

600 where M is the mixing ratio (in ppbv) of CH_4 in the atmosphere, F_{CH4} is the source flux of CH_4
601 to the atmosphere, λ is atmospheric removal rate (1/9 yr^{-1}, assumed for this illustration to be
602 fixed), the *R* terms are the ratio of $^{13}CH_4$ to $^{12}CH_4$, as defined for equation (1), and α_{OH} is the
603 isotopic fractionation (= 0.994, or about -6‰) for atmospheric oxidation of CH_4 by OH[28].
604 Baseline flux to the atmosphere (F_{CH4}) was set to 559 Tg CH_4 the 1980 value[28]. The isotopic
605 composition of CH_4 inputs to the atmosphere (R_{CH4}) were set to the equivalent of -53‰ to allow
606 steady-state modern atmospheric CH_4 to have the observed value of ~ -47‰.

607 We implemented this model numerically in the R software package[48], simulating the
608 effect on the atmosphere of CH_4 emission due to permafrost thaw and partial decomposition of
609 the 1,700 PgC stock of permafrost C anticipated over the next 300 years, as summarized in
610 Schurr et al[2] and Tarnocai et al[1]. High and low permafrost carbon release scenarios for both high
611 (IPCC scenario RCP8.5, leading to release of 120 to 195 PgC) and low (IPCC scenario RCP2.6,
612 approximated as one-third the C release of the high scenario) climate change scenarios
613 (Extended Data Fig. 2a) generated CH_4 emissions (Fig. 3a) (based on 2.3% of released
614 permafrost carbon emerging as CH_4, Schurr et al[2]) and corresponding impacts on the
615 atmospheric concentrations of CH_4 (Extended Data Fig. 3b). We simulated the impacts of these
616 emissions on the isotopic composition of atmospheric CH_4 by assuming the $\delta^{13}C$ of CH_4 emitted
617 was in the range of what we report here for Stordalen Mire, from very light (-80‰, like that
618 measured in the *Sphagnum* site) to only moderately light (-65‰, like that measured in the
619 *Eriophorum* site), giving a range of isotopic perturbations to atmospheric CH_4 under high climate
620 change (Extended Data Fig. 2c) and under low climate change (Extended Data Fig. 2d). In all
621 scenarios, the induced change in atmospheric $\delta^{13}C$ is significantly larger than the atmospheric
622 detection limit of 0.1‰ (reported in Kai et al [28] and shown as a dotted horizontal line in
623 Extended Data Fig. 3c,d).
624 For the analysis shown in Fig. 3, we focused on a mid-range value of permafrost C
625 release (high climate change scenario with low C release, 120 Pg total C by 2100),
626 corresponding to emissions of 2.8 PgC as CH_4 by 2100 (the dashed black-and-red line in Fig.
627 3a). (By comparison, the IPCC estimates that up to 5 PgC may be released as CH_4 by 2100.[3])
628 We explored the mis-attribution of C release that would occur by (mistakenly) assuming that
629 isotopic composition of emitted CH_4 was in the range of assumptions used in previous

atmospheric inversions, from -60‰ to -65‰ [28], instead of the range measured at Stordalen Mire (-65‰ to -80‰). We estimated the magnitude of mis-attribution (or error flux, Fig. 3c) by simulating the amount of additional carbon that would need to be released (at nominally assumed isotopic composition values of -60 or -65) in order to have the same effect on atmospheric composition as the carbon released under scenarios with isotopic compositions like those observed in the field.

References

31. Payette, S. Accelerated thawing of subarctic peatland permafrost over the last 50 years. *Geophysical Research Letters* **31**, 1–4 (2004).

32. O'Donnell, J. a. *et al.* The Effects of Permafrost Thaw on Soil Hydrologic, Thermal, and Carbon Dynamics in an Alaskan Peatland. *Ecosystems* **15**, 213–229 (2012).

33. Vitt, D. H., Halsey, L. A. & Zoltai, S. C. The changing landscape of Canada's western boreal forest: the current dynamics of permafrost. *Canadian Journal of Forest Research* **30**, 283–287 (2000).

34. Quinton, W. L., Hayashi, M. & Chasmer, L. E. Permafrost-thaw-induced land-cover change in the Canadian subarctic: implications for water resources. *Hydrological Processes* **25**, 152–158 (2011).

35. Zoltai, S. C. Cyclic Development of Permafrost in the Peatlands of Northwestern Alberta, Canada. *Arctic and Alpine Research* **25**, 240–246 (1993).

36. Camill, P. & Clark, J. S. Climate change disequilibrium of boreal permafrost peatlands caused by local processes. *The American naturalist* **151**, 207–222 (1998).

37. Dyke, L. D. & Sladen, W. E. Permafrost and Peatland Evolution in the Northern Hudson Bay Lowland, Manitoba. *Arctic* **63**, 429–441 (2010).

38. Whiticar, M. J. & Faber, E. Methane oxidation in sediment and water column environments - Isotopic evidence. *Organic Geochemistry* **10**, 759–768 (1986).

39. Conrad, R. Quantification of methanogenic pathways using stable carbon isotopic signatures: a review and a proposal. *Organic Geochemistry* **36**, 739–752 (2005).

40. Bäckstrand, K., Crill, P. M., Mastepanov, M., Christensen, T. R. & Bastviken, D. Non-methane volatile organic compound flux from a subarctic mire in Northern Sweden. *Tellus B* **60**, 226–237 (2008).

41. Bubier, J. L., Crill, P. M., Mosedale, A., Frolking, S. & Linder, E. Peatland responses to varying interannual moisture conditions as measured by automatic CO_2 chambers. *Global Biogeochemical Cycles* **17**, (2003).

42. Santoni, G. W. *et al.* Mass fluxes and isofluxes of methane (CH_4) at a New Hampshire fen measured by a continuous wave quantum cascade laser spectrometer. *Journal of Geophysical Research* **117**, D10301 (2012).

43. Werle, P., Mücke, R. & Slemr, F. The Limits of Signal Averaging in Atmospheric Trace-Gas Monitoring by Tunable Diode-Laser Absorption Spectroscopy (TDLAS). *Applied Physics B* **139**, 131–139 (1993).

44. Bäckstrand, K., Crill, P. M., Mastepanov, M., Christensen, T. R. & Bastviken, D. Total hydrocarbon flux dynamics at a subarctic mire in northern Sweden. *Journal of Geophysical Research* **113**, (2008).

45. Pataki, D. E. The application and interpretation of Keeling plots in terrestrial carbon cycle research. *Global Biogeochemical Cycles* **17**, (2003).

46. Keeling, C. D. The concentration and isotopic abundances of atmospheric carbon dioxide in rural areas. *Geochimica et Cosmochimica Acta* **13**, 322–334 (1958).

47. Keeling, C. D. The concentration and isotopic abundances of carbon dioxide in rural and marine air. *Geochimica et Cosmochimica Acta* **24**, 277–298 (1960).

48. Team, R. C. R: A language and environment for statistical computing. R Foundation for Statistical Computing. ISBN 3–900051–07–0 (2012).at <http://www.r-project.org/>

49. Corbett, J. E. *et al.* Partitioning pathways of CO_2 production in peatlands with stable carbon isotopes. *Biogeochemistry* **114**, 327–340 (2013).

50. Chanton, J. P., Fields, D. & Hines, M. E. Controls on the hydrogen isotopic composition of biogenic methane from high-latitude terrestrial wetlands. *Journal of Geophysical Research* **111**, 1–9 (2006).

51. Bragg, L., Stone, G., Imelfort, M., Hugenholtz, P. & Tyson, G. W. Fast, accurate error-correction of amplicon pyrosequences. *Nature Methods* **9**, 425–426 (2012).

52. Li, W. & Godzik, A. Cd-hit: a fast program for clustering and comparing large sets of proteins or nucleotide sequences. *Bioinformatics* **22**, 1658–1659 (2006).

690 53. Altschul, H. J. *et al.* Gapped BLAST and PSI-BLAST: A new generation of protein
691 database search programs. *Nucleic Acids Research* **25**, 3389–3402 (1997).

692 54. Caporaso, J. G. *et al.* QIIME allows analysis of high-throughput community sequencing
693 data. *Nature Methods* **7**, 335–336 (2010).

694 55. Ludwig, W. *et al.* ARB: a software environment for sequence data. *Nucleic Acids*
695 *Research* **32**, 1363–71 (2004).

696 56. Conrad, R. The global methane cycle: recent advances in understanding the microbial
697 processes involved. *Environmental Microbiology Reports* **1**, 285–292 (2009).

698 57. Tans, P. P. A note on isotopic ratios and the global atmospheric methane budget. *Global*
699 *Biogeochemical Cycles* **11**, 77–81 (1997).

700

701 **Extended Data Figure and Table Legends:**

702 **Extended Data Figure 1. Expected and observed relationships between δD and $\delta^{13}C$ content**
703 **of porewater CH_4.** The thick gray arrow shows the expected pattern in H and C isotopes of CH_4
704 when variations are caused by shifts between acetoclastic (lower right) and hydrogenotrophic
705 (upper left) production. The thin black arrows pointing to the upper right indicate the expected
706 pattern in H and C isotopes of CH_4 when variations are caused by changes in CH_4 oxidation[19].
707 The points are observed isotopic compositions of samples collected July–October 2011 at the
708 partly thawed *Sphagnum* and fully thawed *Eriophorum* sites, with site averages shown with error
709 bars (error bars represent s.e.m, n = 13 (*Sphagnum*) and 20 (*Eriophorum*)) . Although the scatter
710 allows for some variation in both production and oxidation, the average *Eriophorum* porewater
711 CH_4 had significantly more ^{13}C and less D relative to *Sphagnum* porewater (Hotelling's T^2 Test,
712 $p = 0.0001$), indicating that overall inter-site isotopic differences were due mostly to differences
713 in CH_4 production pathway rather than to differences in CH_4 oxidation. Additionally, in August
714 there was also a significant, negative relationship between $\delta^{13}C$-CH_4 and δD-CH_4 of porewater
715 samples collected across sites (dashed line, $R^2 = 0.5$, $p < 0.02$). Note that on the vertical axis,

716 $\delta D\text{-}H_2O$ has been subtracted from $\delta D\text{-}CH_4$ to correct for the effect of δD exchange between H_2O
717 and CH_4 [20,38,50].
718
719 **Extended Data Figure 2. Simulations, using high and low temperature and C release**
720 **scenarios, of the effect of CH_4 release from thawing permafrost on atmospheric $\delta^{13}C\text{-}CH_4$.**
721 **a,** Scenarios of permafrost C release due to thaw (high temperature, red bounding lines; low
722 temperature, orange bounding lines; with the range in each case defined by high and low C-
723 release scenarios); **b,** Impact on atmospheric methane mixing ratios (assuming 2.3% of released
724 C is emitted as methane); **c,** Impact of high climate change scenario on atmospheric methane
725 isotopes, assuming "*Eriophorum*-like" emissions ($\delta^{13}C \approx -65‰$, blue bounding lines), or
726 assuming "*Sphagnum*-like" emissions ($\delta^{13}C \approx -80‰$, green bounding lines); and **d,** Same as (c),
727 except for low climate change scenario. In (c) and (d) dotted horizontal lines indicate the
728 detection limit for CH_4 isotopes [28].
729
730 **Extended Data Table 1. Summary of porewater chemistry, average (standard error), n=3.**
731
732 **Extended Data Table 2. Relative abundance, taxonomic classification and predicted**
733 **methanogenic pathway of the dominant methanogen operational taxonomic units (OTUs).**
734
735 **Extended Data Table 3. Relative abundance of methanogen functional groups within**
736 **the Archaea**
737 *Above the water table
738 †Below the water table

Extended Data Table 4. Results of linear regression analysis for predicting α_C from relative abundances of methanogenic pathways, dominant methanogenic lineages and environmental variables (n = 41)

*see Extended Data Table 2 for taxonomic details

Extended Data Table 5. Results of stepwise multiple regression analysis for predicting α_C from relative abundances of methanogenic lineages and environmental variables

*see Extended Data Table 2 for taxonomic details

Extended Data Table 6. Estimate of the relative contribution of hydrogenotrophic production to annual CH_4 emission at Stordalen mire

* Based on Johansson et al. [4], the *Sphagnum* site in this study is representative of the Semiwet and Wet vegetation classes.

† Annual total hydrocarbon emissions from Bäckstrand et al. [16] corrected for non-methane volatile organic compound (NMVOC) flux using the reported proportions (25% NMVOC for the *Eriophorum* site, 15% for the *Sphagnum* site). The magnitude of growing season CH_4 emissions measured in this study is comparable to the growing season CH_4 flux used in the Bäckstrand et al. estimate of annual flux.

‡Two approaches: isotopic, using mixing of acetoclastic (-60‰) and hydrogenotrophic (-80‰) sources to yield mean emitted $\delta^{13}C$-CH_4, and molecular, using proportion of the methanogen community identified as hydrogenotrophic.

762 § Molecular approach: on average 86% of methanogen community in the anoxic CH_4-
763 producing peat was identified as hydrogenotrophic, all of the acetoclasts were facultative
764 so this is likely an underestimation of potential hydrogenotrophic production.
765 || Isotopic approach: -79.6‰ ~ -80‰ * **0.98** + -60‰*0.02
766 ¶Isotopic approach: -66.3‰ ~ -80‰*__0.32__ + -60‰*0.68
767 # Molecular approach: on average 62% of the methanogen community was identified as
768 hydrogenotrophic.
769
770 **Extended Data Table 7. SSU rRNA gene amplicon multiplex identifiers (MIDs) used for**
771 **each sample**
772 * Sample names are comprised of the date of sampling, followed by P, S or E for Palsa,
773 *Sphagnum*, or *Eriophorum* sites, respectively, the number indicates the core within the site, and
774 S, M or D indicates surface, middle or deep sampling within the core, respectively.
775 † Samples were multiplexed in six separate runs, each time with samples not related to this study.
776 The multiplex identifiers of the first five runs are given in Mondav et al [6].
777
778 **Extended Data Table 8. Results of stepwise multiple regression analysis for predicting**
779 **δ^{13}C-CH_4 from relative abundances of methanogenic lineages and environmental variables**
780 **(Model 1), the relative abundance of '*M. stordalenmirensis*' from environmental variables**
781 **(Model 2), and α_C from environmental variables (Model 3)**

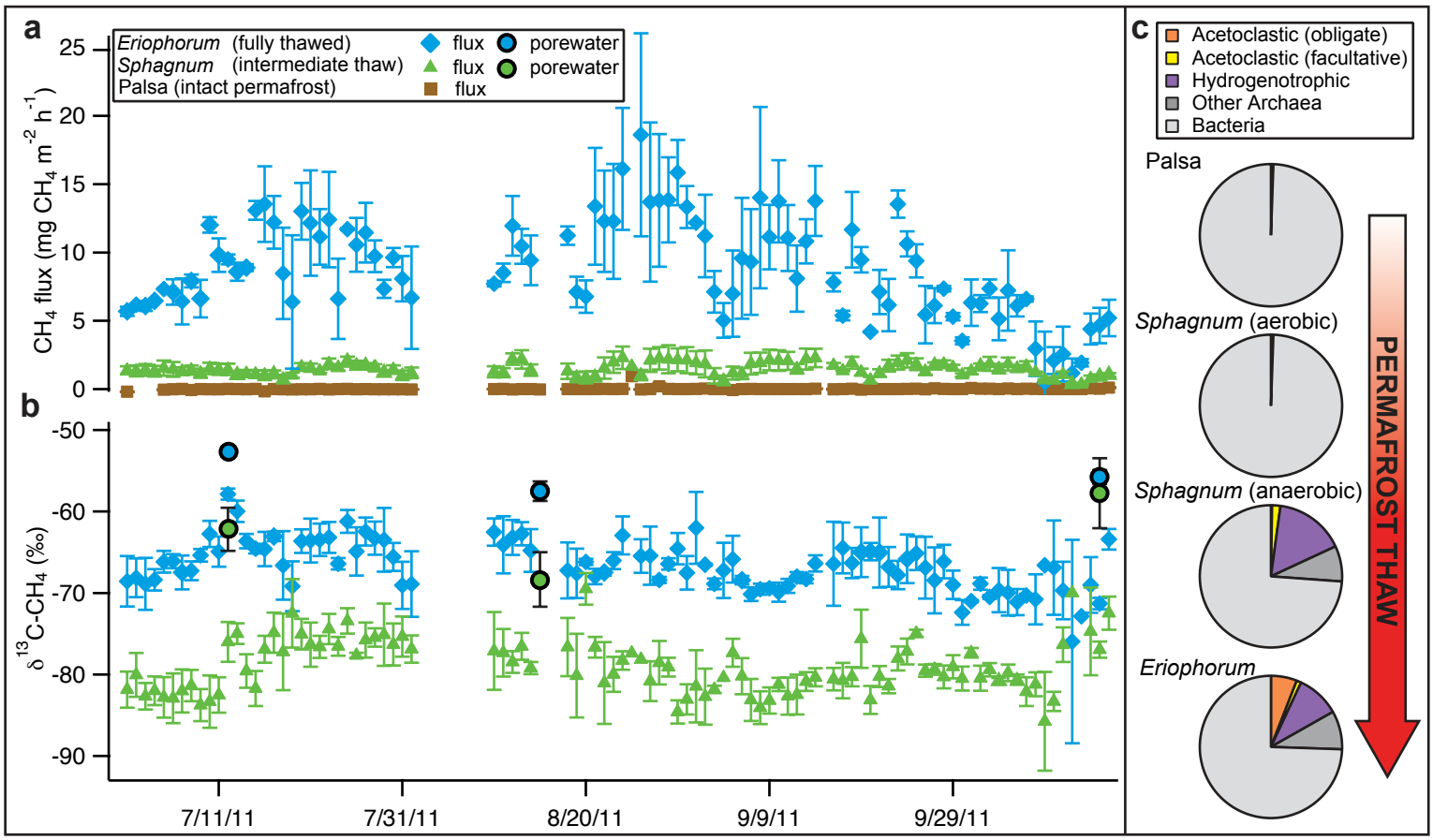
a
Eriophorum (fully thawed)
Sphagnum (intermediate thaw)
Palsa (intact permafrost)
flux
flux
flux
porewater
porewater
CH4 flux (mg CH4 m-2 h-1)
25
20
15
10
5
0
b
δ13C-CH4 (‰)
-50
-60
-70
-80
-90
7/11/11
7/31/11
8/20/11
9/9/11
9/29/11
c
Acetoclastic (obligate)
Acetoclastic (facultative)
Hydrogenotrophic
Other Archaea
Bacteria
Palsa
Sphagnum (aerobic)
Sphagnum (anaerobic)
Eriophorum
PERMAFROST THAW

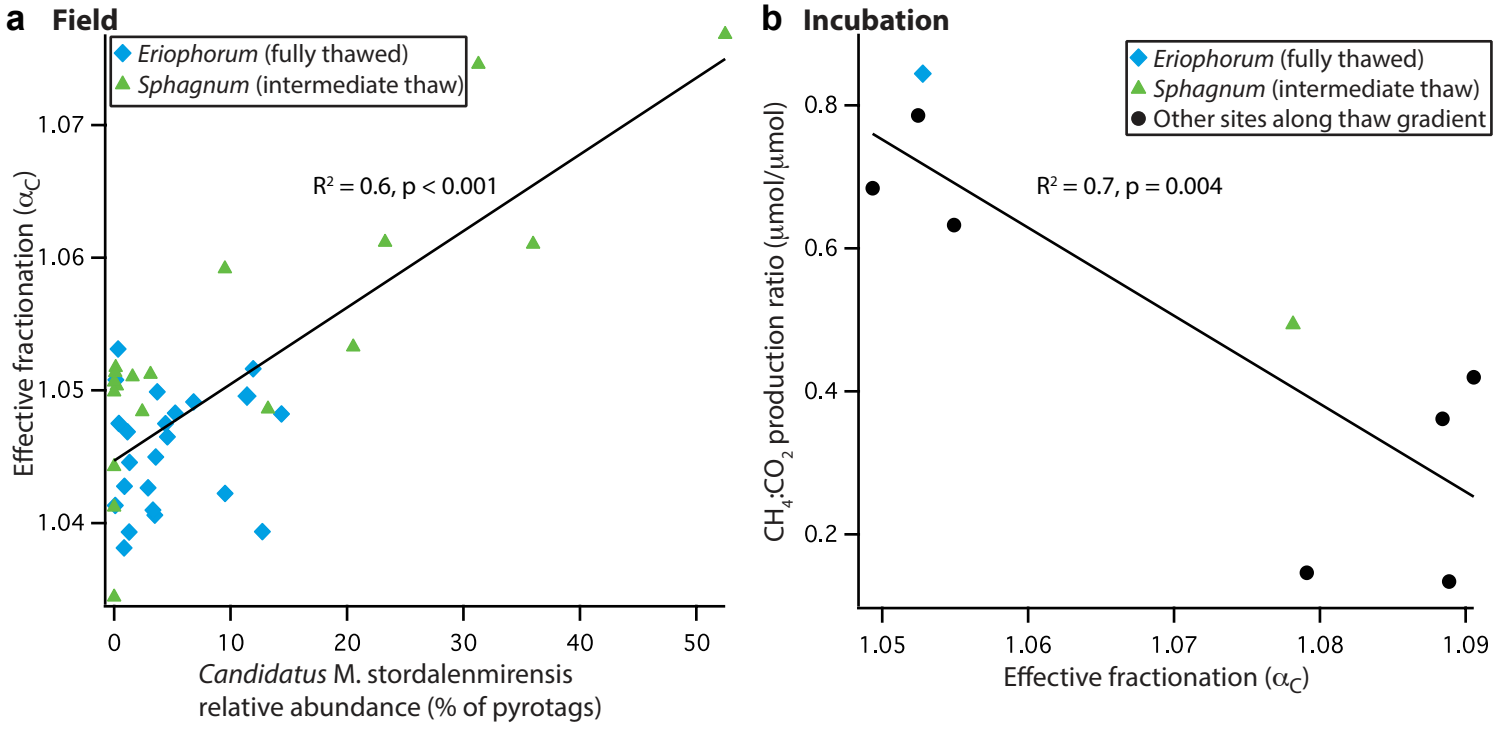
a Field
Eriophorum (fully thawed)
Sphagnum (intermediate thaw)
R² = 0.6, p < 0.001
Effective fractionation (αC)
1.04
1.05
1.06
1.07
0
10
20
30
40
50
Candidatus M. stordalenmirensis
relative abundance (% of pyrotags)
b Incubation
Eriophorum (fully thawed)
Sphagnum (intermediate thaw)
Other sites along thaw gradient
R² = 0.7, p = 0.004
CH4:CO2 production ratio (μmol/μmol)
0.2
0.4
0.6
0.8
1.05
1.06
1.07
1.08
1.09
Effective fractionation (αC)

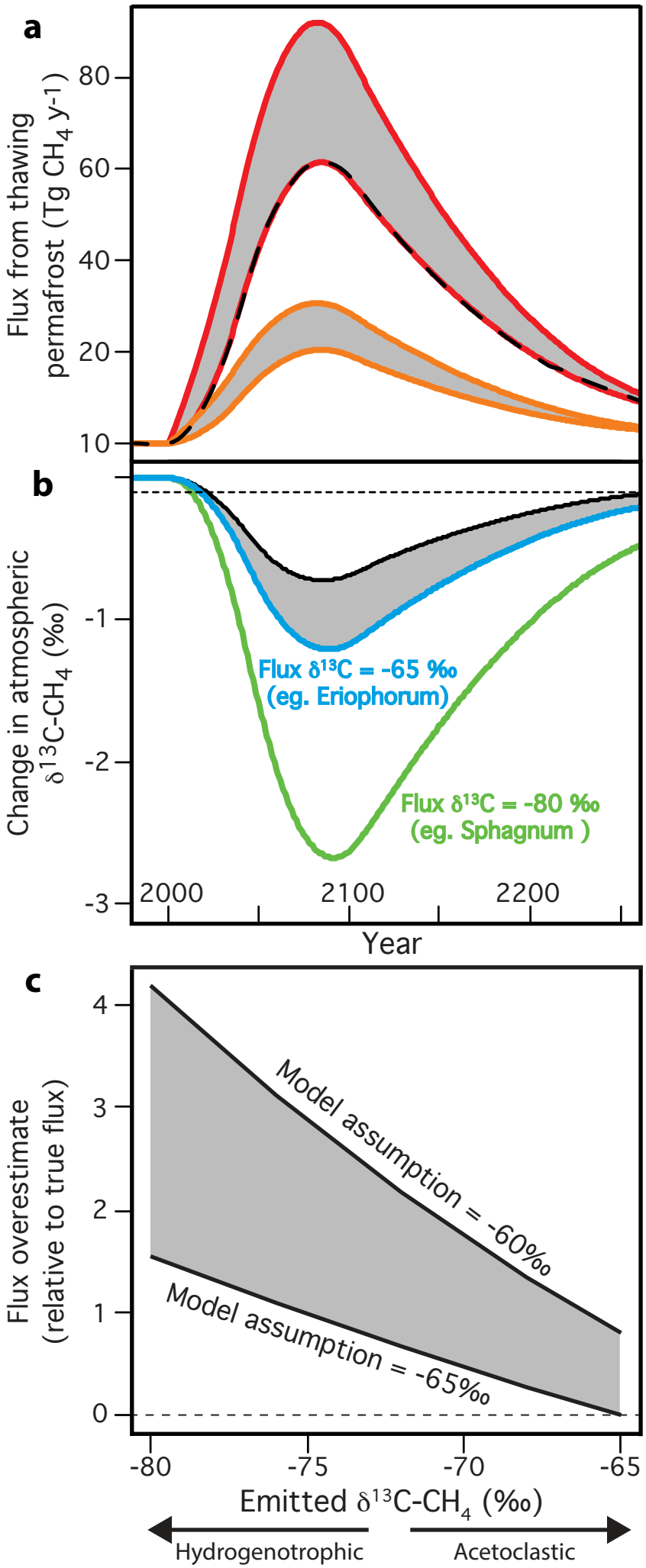
a
Flux from thawing permafrost (Tg CH4 y-1)
80
60
40
20
10
b
Change in atmospheric δ13C-CH4 (‰)
-1
-2
-3
Flux δ13C = -65 ‰
(eg. Eriophorum)
Flux δ13C = -80 ‰
(eg. Sphagnum)
2000
2100
2200
Year
c
Flux overestimate
(relative to true flux)
4
3
2
1
0
Model assumption = -60‰
Model assumption = -65‰
-80
-75
-70
-65
Emitted δ13C-CH4 (‰)
Hydrogenotrophic
Acetoclastic

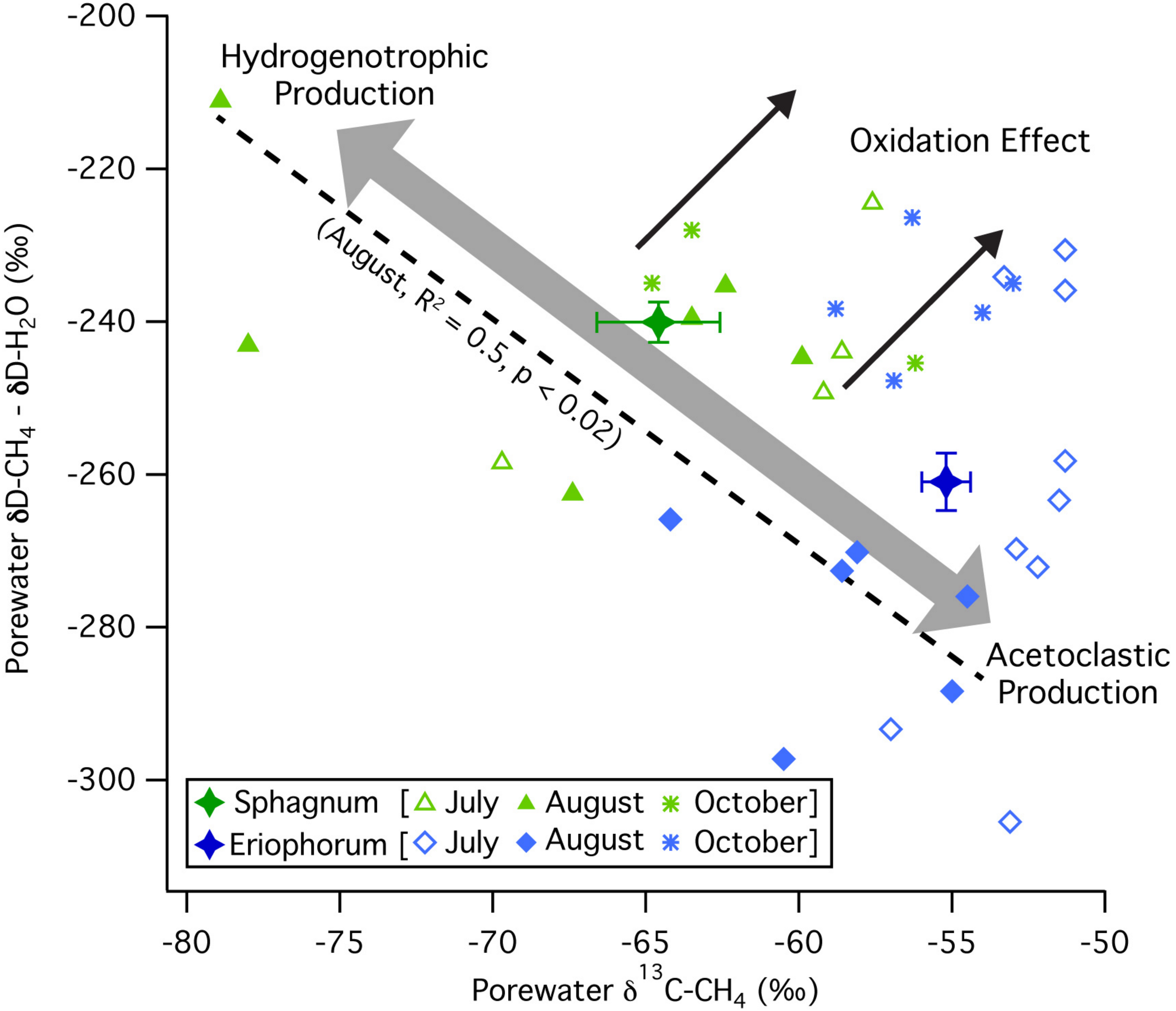
Hydrogenotrophic
Production
Oxidation Effect
(August, R^2 = 0.5, p < 0.02)
Acetoclastic
Production
Sphagnum [July August October]
Eriophorum [July August October]
-200
-220
-240
-260
-280
-300
-80
-75
-70
-65
-60
-55
-50
Porewater δD-CH_4 - δD-H_2O (‰)
Porewater δ^{13}C-CH_4 (‰)

a

Permafrost carbon (Pg)

1000 1200 1400 1600

2000 2100 2200

b

Change in atmospheric CH_4 (ppb)

0 50 100 150 200 250

2000 2100 2200

c

Change in atmospheric $\delta^{13}C\text{-}CH_4$ (‰)

0 −1 −2 −3 −4

2000 2100 2200

Year

d

Change in atmospheric $\delta^{13}C\text{-}CH_4$ (‰)

0 −1 −2 −3 −4

2000 2100 2200

Year

Sample	Depth (cm)	pH	mM CO_2	mM CH_4	$\delta^{13}CO_2$ ‰	$\delta^{13}CH_4$ ‰	α_C
July, 2011							
Sphagnum - M	13	4.1 (0.06)	3.02 (0.78)	0.09 (0.04)	-15.7 (1.6)	-62.2 (3.8)	1.050 (0.005)
Sphagnum - D	19	4.2 (0.09)	3.50 (0.57)	0.15 (0.05)	-14.1 (0.6)	-62.2 (4.5)	1.051 (0.005)
Eriophorum - S	3	5.8 (0.09)	2.29 (0.92)	0.18 (0.12)	-14.1 (1.1)	-52.1 (0.5)	1.040 (0.001)
Eriophorum -M	7	5.6 (0.06)	3.06 (0.77)	0.28 (0.07)	-12.9 (1.0)	-52.6 (0.6)	1.042 (0.001)
Eriophorum - D	24	5.6 (0.03)	3.56 (0.80)	0.36 (0.07)	-11.6 (1.7)	-53.3 (1.9)	1.044 (0.004)
August, 2011							
Sphagnum - M	21	4.2 (0.10)	4.89 (0.37)	0.23 (0.04)	-12.0 (1.5)	-66.7 (5.7)	1.059 (0.008)
Sphagnum - D	26	4.1 (0.13)	4.80 (0.48)	0.23 (0.04)	-10.7 (1.6)	-69.9 (4.6)	1.064 (0.007)
Eriophorum - S	3	5.7 (0.19)	1.62 (0.28)	0.06 (0.04)	-13.5 (0.5)	-60.0 (2.6)	1.049 (0.003)
Eriophorum -M	7	5.7 (0.10)	1.93 (0.25)	0.10 (0.02)	-13.9 (0.4)	-56.6 (2.1)	1.045 (0.002)
Eriophorum - D	26	5.6 (0.15)	3.58 (0.62)	0.31 (0.11)	-11.1 (2.4)	-55.9 (1.1)	1.047 (0.001)
October, 2011							
Sphagnum - M	10	4.3 (0.06)	1.24 (0.42)	0.03 (0.02)	-16.4 (1.6)	-59.2 (6.5)	1.046 (0.006)
Sphagnum - D	15	4.5 (0.10)	3.21 (0.90)	0.10 (0.04)	-13.8 (2.4)	-61.5 (2.7)	1.051 (0.0004)
Eriophorum - S	3	5.9 (0.15)	2.15 (1.43)	0.19 (0.13)	-14.1 (1.0)	-56.4 (2.4)	1.045 (0.001)
Eriophorum -M	7	5.9 (0.15)	2.71 (1.25)	0.29 (0.14)	-13.7 (1.6)	-57.8 (3.1)	1.047 (0.002)
Eriophorum - D	26	5.7 (0.12)	3.84 (1.64)	0.53 (0.27)	-11.3 (3.1)	-58.1 (2.2)	1.050 (0.001)

Sample	Candidatus *Methanoflorens* (otu-10747) Hydrogenotrophic	*Methanobacterium* (otu-3636) Hydrogenotrophic	Candidatus *Methanoregula* (otu-20819) Hydrogenotrophic	*Methanosarcina* (otu-7308) Acetoclastic (facultative)	*Methanosaeta* (otu-10220) Acetoclastic (obligate)	*Methanosaeta* (otu-15150) Acetoclastic (obligate)
July, 2011						
Palsa – S	0.0	0.0	0.0	0.0	0.0	0.0
Palsa – M	0.0	0.0	0.0	0.0	0.0	0.0
Palsa – D	0.0	0.4	0.0	0.0	0.0	0.0
Sphagnum – S	0.3	0.4	0.0	0.1	0.0	0.0
Sphagnum – M	4.0	12.9	0.0	3.4	0.0	0.0
Sphagnum – D	16.4	5.8	0.0	3.3	0.0	0.0
Eriophorum – S	1.0	2.7	5.8	0.7	4.5	1.8
Eriophorum – M	5.3	3.7	4.0	2.2	5.0	2.7
Eriophorum – D	8.3	1.6	1.9	0.6	4.2	1.2
August, 2011						
Palsa – S	0.0	0.0	0.0	0.0	0.0	0.0
Palsa – M	0.0	0.0	0.0	0.0	0.0	0.0
Palsa – D	0.0	0.0	0.0	0.0	0.0	0.0
Sphagnum – S	0.1	0.4	0.0	0.2	0.0	0.0
Sphagnum – M	11.6	4.0	0.0	1.9	0.0	0.0
Sphagnum – D	32.1	3.1	0.0	1.4	0.0	0.0
Eriophorum – S	0.6	2.1	3.6	0.4	3.3	1.0
Eriophorum – M	6.3	6.1	5.1	2.6	9.0	3.9
Eriophorum – D	6.5	0.3	3.4	1.2	1.7	0.6
October, 2011						
Palsa – S	0.0	0.0	0.0	0.0	0.0	0.0
Palsa – M	0.1	1.1	0.0	0.1	0.0	0.0
Palsa – D	0.1	0.7	0.0	0.0	0.0	0.0
Sphagnum – S	0.0	0.1	0.0	0.0	0.0	0.0
Sphagnum – M	0.0	3.4	0.0	1.1	0.0	0.0
Sphagnum – D	0.6	8.4	0.0	1.2	0.0	0.0
Eriophorum – S	2.5	1.7	1.7	0.6	1.4	0.6
Eriophorum – M	2.1	1.9	1.0	0.8	2.5	2.2
Eriophorum – D	6.0	1.1	3.7	0.1	5.1	5.8

Site	Hydrogenotrophic	Acetoclastic (facultative)	Acetoclastic (obligate)	Other Archaea
July, 2011				
Palsa	35.9	2.9	0.0	61.2
Sphagnum (aerobic)*	83.1	15.5	0.0	1.4
Sphagnum (anaerobic)†	82.1	14.2	0.0	3.8
Eriophorum	39.5	4.2	21.4	34.9
August, 2011				
Palsa	0.0	8.7	0.0	91.3
Sphagnum (aerobic)*	68.2	30.7	0.0	1.1
Sphagnum (anaerobic)†	91.2	6.1	0.0	2.8
Eriophorum	39.5	5.1	21.9	33.5
October, 2011				
Palsa	56.5	2.6	0.4	40.5
Sphagnum (aerobic)*	65.7	24.0	0.7	9.6
Sphagnum (anaerobic)†	15.6	2.8	2.6	79.0
Eriophorum	35.8	2.4	27.6	34.2

Variable	R^2	F-statistic	p-value
'*M. stordalenmirensis*'	0.58	54.09	<0.001
otu-3636*	0.00	0.01	0.926
otu-10220*	0.12	5.36	0.026
otu-20819 *	0.15	6.82	0.013
otu-15150 *	0.06	2.27	0.140
otu-7308 *	0.01	0.32	0.576
Hydrogenotrophic	0.44	30.63	<0.001
Acetoclastic (obligate)	0.12	5.23	0.028
Water table depth	0.44	31.1	<0.001
pH	0.19	8.97	0.005
Porewater CH_4 (mM)	0.00	0.07	0.796
Porewater DIC (mM)	0.25	13.33	0.001
Peat C:N	0.00	0.17	0.682
Peat %C	0.02	0.75	0.393
Peat %N	0.00	0.14	0.709
Peat $\delta^{13}C$	0.13	5.99	0.019

Variable	Coefficient	Std Error	t value	p value	Cumulative AIC
Model 1 - stepwise regression, direction = both (R^2 = 0.81, F = 23.71 on 6 and 34 df, p <0.001)					
Water table depth	-0.0004	0.0001	-5.398	<0.001	-422.33
'*M. stordalenmirensis*'	0.0271	0.0084	3.221	0.002	-436.79
C:N	-0.0002	0.0001	-2.872	0.007	-438.80
Peat $\delta^{13}C$	0.0014	0.0006	2.516	0.017	-440.71
DIC (mM)	0.0007	0.0005	1.396	0.171	-445.42
otu-3636*	-0.0271	0.0161	-1.345	0.188	-445.58
Intercept	1.089	0.0167	65.193	<0.001	-445.71
Model 2 – significant predictor variables from model 1 (R^2 = 0.79, F = 33.71 on 4 and 36 df, p <0.001)					
Water table depth	-0.0004	0.0001	-5.202	<0.001	-425.11
'*M. stordalenmirensis*'	0.0351	0.0072	4.867	<0.001	-427.36
C:N	-0.0002	0.0001	-2.613	0.013	-440.97
Peat $\delta^{13}C$	0.0014	0.0006	2.470	0.018	-441.67
Intercept	1.089	0.0164	66.583	<0.001	-446.09

Habitat	Area (ha)*	Annual Flux (g CH_4 m^{-2}) †	Annual Emission (kg CH_4) *,†	Estimated Emission from Hydrogenotrophy (kg CH_4 yr^{-1}) ‡
Sphagnum	6.2	6.2	288.3	247.9§ - 282.5‖
Eriophorum	2.0	36.0	540.6	172.8¶– 335.2#
Total			828.9	420.7(51%) – 617.7 (75%)

Sample name	Run #	Multiplex identifier (MID)
20110712_E_3_M	6	CGAGC
20110712_S_1_M	6	CGCAT
20110712_S_3_M	6	CGTAC
20110712_P_1_S	6	CGTGT
20110712_P_2_S	6	CTAGT
20110712_P_3_S	6	CTGAC
20110816_S_2_S	6	TACGC
20110816_S_1_D	6	TATGT
20110816_P_1_M	6	TCAGT
20111016_P_1_S	6	TCGAT

Variable	Coefficient	Std Error	t value	p value	Cumulative AIC
Model 1 - stepwise regression, dependent variable = δ^{13}C-CH_4, direction = both (R^2 = 0.75, F = 21.25 on 5 and 35 df, p <0.001)					
Water table depth	0.299	0.07	4.512	<0.001	130.95
'*M. stordalenmirensis*'	-23.25	6.79	-3.426	0.002	124.01
Peat δ^{13}C	-1.51	0.54	-2.779	0.009	120.33
CH_4 (mM)	10.60	4.12	2.576	0.014	119.28
C:N	0.12	0.05	2.149	0.039	117.24
Intercept	-102.14	15.23	-6.705	<0.001	114.16
Model 2 - stepwise regression, dependent variable = '*M stordalenmirensis*', direction = both (R^2 = 0.53, F = 7.77 on 5 and 35 df, p <0.001)					
Water table depth	-0.0053	0.0015	-3.634	<0.001	-188.03
C:N	-0.0035	0.0010	-3.495	0.001	-188.88
DIC (mM)	0.0214	0.0106	2.025	0.050	-196.61
% C	0.0033	0.0018	1.799	0.081	-197.53
Soil temperature	0.0059	0.0040	1.483	0.147	-198.66
Intercept	-0.0558	0.0805	-0.692	0.493	-199.15
Model 3 - stepwise regression, dependent variable = α_c, direction = both (R^2 = 0.71, F = 21.71 on 4 and 36 df, p <0.001)					
Water table depth	-0.0005	0.0001	-6.465	<0.001	-402.97
C:N	-0.0003	0.0001	-4.514	<0.001	-416.18
DIC (mM)	0.0015	0.0006	2.629	0.013	-427.36
Peat δ^{13}C	0.0017	0.0007	2.574	0.014	-427.63
Intercept	1.0990	0.0192	57.396	<0.001	-432.56